An alternative approach to the kinetic modeling of pharmaceuticals degradation in high saline water by electrogenerated active chlorine species

Ruth F. Flores-Terreros [1], Efraím A. Serna-Galvis [2,3], Javier Navarro-Laboulais [4], Ricardo A. Torres-Palma [3,*] and Jessica I. Nieto-Juárez [1,*]

[1]*Research Group in Environmental Quality and Bioprocesses (GICAB), Faculty of Chemical Engineering and Textile, Universidad Nacional de Ingeniería UNI, Av. Túpac Amaru No 210, Rímac, Lima, Perú.*

[2]*Grupo de Investigación en Remediación Ambiental y Biocatálisis (GIRAB), Instituto de Química, Facultad de Ciencias Exactas y Naturales, Universidad de Antioquia UdeA, Calle 70 No. 52-21, Medellín, Colombia.*

[3]*Grupo de Investigaciones Biomédicas Uniremington, Facultad de Ciencias de la Salud, Corporación Universitaria Remington (Uniremington), Calle 51 No. 51-27, Medellín, Colombia.*

[4]*Department of Chemical and Nuclear Engineering, Universitat Politècnica de València, Camino de Vera s/n, 46022 Valencia, Spain.*

*Correspondence: ricardo.torres@udea.edu.co (R.A.T-P.); jnieto@uni.edu.pe (J.I.N-J.)

Abstract

Kinetic modeling contributes to understand fundamental and practical aspects of pharmaceuticals degradation in water by electrogenerated reactive chlorine species (RCS). Herein, a different approach to those in literature for the modeling of acetaminophen (ACE) degradation by the RCS is presented. A filter-press reactor having a dimensionally stable anode, NaCl, and operated in continuous mode, was considered, where high current (100 mA) and low flow (11 mL min^{-1}) favored the electrogeneration of RCS used for ACE degradation. A semi-empirical kinetic model considering the rate of RCS production (Φ_E) as a function of current intensity and chloride concentration was developed. The model successfully reproduced the ACE removal at different concentrations (10, 20, 40, and 60 mg L^{-1}) in distilled water. Φ_E and hydraulic retention time were the most relevant parameters of the model for the generation of RCS, and these two parameters plus the pollutant concentration were very determinant on ACE degradation. Also, the treatment of ACE in actual seawater was assessed and simulated. The competing role toward electrogenerated RCS by intrinsic organic matter in the seawater was a key point, and the simulated values fitted well to the experimental ones. Finally,

the action of the electrochemical system on ciprofloxacin (CIP) in the real seawater and the evolution of its antimicrobial activity were tested. CIP removal was faster than that observed for ACE due to structural differences between both pharmaceuticals. Moreover, the system removed the antimicrobial activity associated with CIP, indicating a positive effect regarding the impact of pharmaceuticals in environmental water.

Keywords: Acetaminophen; Electrochemical process; Degradation simulation; Organic pollutants elimination; Reactive chlorine, Water treatment.

1. Introduction

Nowadays, the pharmaceuticals (such as the analgesic acetaminophen or the antibiotic ciprofloxacin) in aquatic ecosystems have fostered great attention in the world due to their persistence and eco-toxicological or environmental risks [1–3]. Their occurrence in water resources, even at low concentrations (ng L^{-1} or µg L^{-1}) generates a potential threat to the environment and public health [4,5]. For example, the bioaccumulation of acetaminophen (ACE) induces inhibition of reproduction and cell growth [2, 8]. Antibiotics like ciprofloxacin (CIP) can cause negative effects, such as the development of antibiotic-resistant bacteria [6, 7]. In addition to the above-mentioned concerns, conventional methods in the mu-

nicipal wastewater treatment plants (WWTP) are not able to eliminate pharmaceuticals [9]. Therefore, efficient treatment methods to ensure the degradation of these problematic substances are needed.

Electrochemical oxidation processes based on the production and action of reactive chlorine species (RCS) are an alternative to degrade pharmaceuticals [11-15]. Dimensionally stable anodes (DSA) are the best anodes for the formation of RCS ($Cl_2, E°$: 1.36 V; $HOCl$, $E°$: 1.49 V; and $OCl^-, E°$: 0.89 V) [10, 11]. Indeed, some works have been focused on kinetic mathematical modeling for the prediction of the oxidation of organic compounds with electro-generated RCS using DSA. The most common models are based on the solution of Nernst-Planck, Navier-Stokes, and reaction-dispersion equations alone or combined in 3D, 2D or 1D coupled with homogeneous and heterogeneous chemical reactions [14–16]. However, these models are very complex in their formulation and number of parameters. A different approach, few studied for processes based on DSA, is the use of semiempirical macroscopic models for application to the electrochemical reactor, which have a limited number of parameters, allowing easy handling of the modeled system. The main advantage of this kind of modeling is that the number of parameters needed to run and simulate the reactor behavior is significantly less than the modeling based on computational fluid dynamics (CFD) but it should be recalibrated when the operation conditions are changed.

Therefore, this research work aims to study the degradation of a relevant pharmaceutical (ACE) by *in situ* electrochemically generated RCS with a DSA, applying a semi-empirical model. The electrochemical system consisted of a laboratory-scale filter press reactor, equipped with a Ti/RuO_2-ZrO_2 (Sb_2O_3 doped) anode, which was chosen because it produces the highest amount of RCS compared to other DSA anodes [17]. Firstly, the effect of two main operational parameters (current intensity and flow) of the reactor on the generation of RCS was evaluated through a surface response analysis. Then, the degrading action of the electrochemical system on ACE was assessed. Afterward, the kinetic model was developed considering the rate of RCS production (Φ_E) as a function of current intensity and chloride concentration. Besides, the sensitivity analysis of the model was performed to calculate the accuracy of the parameters evaluated from experimental data. Additionally, the feasibility of the process on the degradation of ACE in actual seawater was tested, and then it was simulated. Finally, to determine the action of the electrochemical system on other pharmaceuticals, the antibiotic CIP was treated in real seawater and the evolution of its antimicrobial activity was also followed.

2. Materials and Methods

2.1. Reagents

Acetaminophen (ACE) and ciprofloxacin (CIP) were provided by Laproff laboratories (Colombia). Potassium iodide and ammonium heptamolybdate, acetonitrile, and sodium chloride were purchased from Merck. Formic acid was obtained from Carlo Erba. The pharmaceutical solutions were prepared using distilled water. Also, a sample of actual seawater from the Pacific Ocean was considered, and this matrix was spiked with the pharmaceuticals before the experiments.

2.2. Reaction system

Experiments were performed in a filter-press reactor (Fig. S1 in Supporting information), operated in continuous mode, equipped with a DSA (Ti/RuO_2-ZrO_2 (Sb_2O_3 doped)) and a cathode of titanium. The cathode and anode were rectangular plates, with a geometric area of 40 cm^2 (width 2 cm, length 20 cm). The distance between electrodes was 1.5 cm. The electrochemical cell had 60 mL of internal capacity and the supporting electrolyte was sodium chloride. Experiments were done at least by duplicate and aliquots were sampled periodically for the analyses.

2.3. Analyses

The effect of current intensity and flow on the generation of RCS in the electrochemical system was evaluated through the response surface methodology using

Design-Expert 12 software (free trial version). A two-level factorial design with two central points was applied (Table S1). The current intensity (I) was evaluated in the range 20 - 100 mA, and flow (Q) was tested in the range 11 - 50 mL min^{-1}. The response factor was the production of RCS (in µmol L^{-1}) in the absence of pharmaceuticals. The electrogenerated reactive chlorine species were determined by the iodometric method detailed in the reference [18]. The absorbance was recorded at 350 nm after 5 minutes of reaction using a spectrophotometer UV/Vis (Mettler Toledo, UV5).

The degradations of the target pharmaceuticals were performed at the suitable operational conditions of current and flow obtained from the experimental design. The degradations of the pharmaceuticals were quantified using a UHPLC Thermo Scientific Dionex Ultimate 3000 Instrument. A C-18 Thermo Scientific acclaim column (5 µm d.p., 4.6 mm i.d., and 150 mm length) and a diode array detector were used. The phase mobile was a mixture of acetonitrile and formic acid buffer (pH 3.0) 15:85 v/v, and an injection volume of 25 µL. In the case of ACE, a flow rate of 0.45 mL min^{-1} and 243 nm of detection wavelength were used. Meanwhile, for CIP, 0.60 mL min^{-1} and 278 nm were the flow, and detection wavelength, respectively [19].

The actual seawater was characterized using the methods reported in Table S2. Antimicrobial activity (AA) was determined by the inhibition halo method using

Staphylococcus aureus (ATCC 6538) as the indicator microorganism [19]. Antibiotic solution (30 µL) was added to Petri dishes containing 10 mL of nutrient agar inoculated with 10 µL of the bacteria (optical density of 0.600 at 580 nm). The Petri dishes were incubated at 37 °C for 24h in a HeraTherm Thermo Scientific Incubator. Confluent bacterial growth was observed, and the diameter of the inhibitory halo (mm) was measured using a vernier at different treatment times.

2.4. Reactor modeling

The kinetic model was based on a mass balance analysis [20], in which the electrochemical reactor is considered as a continuous stirred tank reactor (CSTR), of batch type and complete mix. From a macroscopic point of view, the chemistry of the oxidation of organic drugs with electrogenerated RCS in a two-electrode electrochemical cell can be represented by the following set of chemical reactions (Table 1, R1-R8):

Table 1. Reactions involved in the electrochemical system.

Component of the system	Reaction	Name
Anode	$2\,Cl^- \xrightarrow{k_{E1}(I)} Cl_2 + 2\,e^-$	R1
	$2\,H_2O \xrightarrow{k_{E2}} O_2 + H^+ + 4\,e^-$	R2
Solution	$Cl_2 + H_2O \xrightarrow{k_1} HOCl + HCl$	R3

	$HOCl \overset{K_a}{\rightleftharpoons} OCl^- + H^+$	R4
	$ACE \overset{K_A}{\rightleftharpoons} ACE^- + H^+$	R5
	$HOCl + ACE \xrightarrow{k_2} Prds.$	R6
	$HOCl + ACE^- \xrightarrow{k_3} Prds.$	R7
Cathode	$2\,H_2O + 2\,e^- \xrightarrow{k_{CAT}} 2\,OH^- + H_2$	R8

The first two reactions in Table 1 are the macroscopic simplification of the mechanism of electrogenerated RCS and the oxygen evolution reaction (OER) respectively proposed by Palma-Goyes [17]. Instead, a detailed description of the mechanism which involves at least three chemical and two electrochemical rate constants, all the reactions are lumped in a single chemical reaction characterized by observable rate coefficients, k_{E1} and k_{E2}, respectively. Both observable rate coefficients depend on the electron transfer rate constants and the adsorption chemistry of the electrogenerated RCS and OER. For simplicity and considering that the chloride ion is in excess, the chlorine production rate is assumed first order for the chloride and will be a source term named Φ_E, the chlorine electrochemical source, or the chlorine rate formation (Eq. 1).

$$\Phi_E = R_{Cl_2} = k_{E1} \cdot C^0_{Cl^-} \tag{1}$$

To solve first the mass balances regarding the chlorine species, given by the reactions R1-R4 and R8. The mass balance for the Cl_2 and OH^- can be written as follows (Eqs. 2-4):

$$\frac{dC_{Cl2}}{dt} = \frac{-q}{V_R} C_{Cl2} + R_{Cl_2} - k_1 \cdot C_{Cl2} \tag{2}$$

$$\frac{dC_{HOCl}}{dt} = \frac{-q}{V_R} C_{HOCl} + k_1 \cdot C_{Cl2} \tag{3}$$

$$\frac{dC_{OH}}{dt} = \frac{q}{V_R}\left(C_{OH}^0 - C_{OH}\right) + R_{OH} - k_1 \cdot C_{Cl2} \tag{4}$$

The first term in the above equations is the input-output term for each species. The R_{Cl_2} and R_{OH} terms are the chlorine and hydroxyl ion production rates for the electrochemical reactions R1 and R8, respectively.

Because the configuration of the electrochemical reactor is the two-electrode in an undivided mode we have that the anodic (I_{AN}) and the cathodic (I_{CAT}) currents must be equal ($I_{AN} = -I_{CAT}$). There are two contributions for the anodic current, one for the chloride oxidation (I_{A1}) corresponding to reaction (R1) and the other one for the water oxidation (I_{A2}) corresponding to reaction (R2). We can define the chlorine current ratio (η) as the current fraction used in chloride oxidation, as presented in Eq. 5.

$$\eta = \frac{I_{A1}}{I_{AN}} = \frac{I_{A1}}{I_{A1} + I_{A2}} \tag{5}$$

Considering the reaction rates of formation for Cl_2 obey first-order reaction respect the chloride concentration and zero-order for the OH^- formation, we have Eqs 6-7.

$$R_{Cl_2} = k_{E1} \cdot C_{Cl^-} = \frac{\eta \cdot I_{AN}}{nF \cdot A} \tag{6}$$

$$R_{OH} = k_{CAT} = \frac{|I_{CAT}|}{nF \cdot A} \tag{7}$$

Then, the formation rate for the chlorine and hydroxyl ions is proportional with $0 < \eta < 1$ (Eq. 8).

$$R_{Cl_2} = \eta \cdot R_{OH} \tag{8}$$

The set of ordinary differential equations (ODE, Eqs. 2-4) can be written in dimensionless form as presented in Eqs. 9-11:

$$\frac{dz}{dt} = k'\left(1 - z\right) \quad ; \quad z(0) = 0 \tag{9}$$

$$\frac{dx}{dt} = \tau_H^{-1}\left(z - x\right) \quad ; \quad x(0) = 0 \tag{10}$$

$$\frac{dw}{dt} = \tau_H^{-1}\left(1 - w\right) + \frac{\Phi_E}{\eta\, C_{OH}^0} - \frac{k_1\, \Phi_E}{k'\, C_{OH}^0}\, z \quad ; \quad w(0) = 1 \tag{11}$$

Where the dimensionless state variables are defined in Eq. 12.

$$z = \frac{k'}{\Phi_E} C_{Cl_2} \quad ; \quad x = \frac{k'}{\tau_H\ k_1\ \Phi_E} C_{HOCl} \quad ; \quad w = \frac{C_{OH}}{C_{OH}^0} \tag{12}$$

With the hydraulic retention time $\tau_H = V_R/q$ and the constant $k' = k_1 + \tau_H^{-1}$.

The set of ODEs is lineal for the state variables and then integrable. For the dimensionless chlorine and hypochlorous acid concentrations, the solution is represented by Eqs. 9-11 gives Eqs. 13 and 14.

$$z(t) = 1 - \exp(-k' t) \tag{13}$$

$$x(t) = 1 - \frac{e^{-k' t} - k' \tau_H e^{-\tau_H^{-1} t}}{1 - k' \tau_H} \tag{14}$$

The hydrolysis constant k_1 is usually several orders of magnitude higher the inverse of the hydraulic retention time and then the dimensionless OH concentration can be expressed by Eq. 15.

$$w(t) = 1 + \frac{\Phi_E \tau_H}{C_{OH}^0 (k_1 \tau_H - 1)} \left[(k_1 \tau_H - 1) X + (1 + X - k_1 \tau_H X) e^{-\tau_H^{-1} t} - e^{-k_1 t} \right] \tag{15}$$

Where $X = \eta^{-1} - 1$. Under these circumstances, the observable variables of the electrochemical system can be expressed as:

$$C_{Cl_2}(t) = \frac{\Phi_E}{k_1} \left(1 - e^{-k_1 \cdot t}\right) \tag{16}$$

$$C_{HOCl}(t) = \tau_H \Phi_E \left(1 - e^{-\tau_H^{-1} \cdot t}\right) \tag{17}$$

$$pH(t) = pH_0 + \log\left(w(t)\right) \tag{18}$$

Thereby, Eq. 17 is particularly useful for calibration purposes and the determination of Φ_E.

In the presence of pharmaceuticals such as acetaminophen (ACE), the set of Eqs. 2-4 must be extended including the reactions R5-R7, as detailed in Eqs. 19-22.

$$\frac{dC_{Cl2}}{dt} = -\tau_H^{-1} C_{Cl2} + \Phi_E - k_1 \cdot C_{Cl2} \tag{19}$$

$$\frac{dC_{HOCl}}{dt} = -\tau_H^{-1}\, C_{HOCl} + k_1 \cdot C_{Cl2} - k_2\, C_{HOCl}\, C_A \tag{20}$$

$$\frac{dC_A}{dt} = \tau_H^{-1}\left(C_{A0} - C_A\right) - k_2\, C_{HOCl}\, C_A \tag{21}$$

$$\frac{dC_{OH}}{dt} = \tau_H^{-1}\left(C_{OH}^0 - C_{OH}\right) + \frac{\Phi_E}{\eta} - k_1 \cdot C_{Cl2} \tag{22}$$

Where C_A is the ACE concentration. Because of the non-linear terms in Eqs. 20 and 21, it is unfeasible to have under these new circumstances an analytical solution such as Eqs. 16-18. In dimensionless units, the set of Eqs. 19-22 can be expressed by Eqs. 23-26.

$$\frac{dz}{dt} = k'\left(1 - z\right) \quad ; \quad z(0) = 0 \tag{23}$$

$$\frac{dx}{dt} = \tau_H^{-1}\left(z - x\right) - C_{A0}\, k_2\, x\, y \quad ; \quad x(0) = 0 \tag{24}$$

$$\frac{dy}{dt} = \tau_H^{-1}\left(1 - y\right) - \tau_H \Phi_E\, k_2\, x\, y \quad ; \quad y(0) = 1 \tag{25}$$

$$\frac{dw}{dt} = \tau_H^{-1}\left(1 - w\right) + \frac{\Phi_E}{\eta\, C_{OH}^0} - \frac{k_1\, \Phi_E}{k'\, C_{OH}^0} \cdot z \quad ; \quad w(0) = 1 \tag{26}$$

Where k_2 is the rate constant between the HOCl and the ACE, and the new state variable $y = {C_A}/{C_{A0}}$.

For the derivation of Eqs. 23-26 the rate constant k_2 has been considered independent of the pH. But there are pieces of evidence of the pH dependence for the reaction between the ACE and the HOCl [21]. The reaction rate constant between the HOCl and the protonated ACE is 3.1 M^{-1} s^{-1} [21], while the reaction rate between the HOCl and the unprotonated ACE is 7×10^3 M^{-1} s^{-1} [21]. The same authors affirm that the OCl- does not react appreciably with the protonated or

unprotonated acid. Under these circumstances, it is possible to define an apparent rate constant for the HOCl/ACE reaction shown in Fig. S2A. The maximum apparent rate constant k_2, app, i.e., 42.4 M^{-1} s^{-1}, is attained at pH = 8.6 according to Eq. 27. Together, it is shown in Fig. S2B, the predominance diagram for the Cl_2/HOCl/OCl^- system with the ACE acid-base diagram.

Because the apparent rate constant between the ACE and the HOCl depends on the pH, and because the pH changes with time, it is necessary to change the constant k_2 in Eqs. 24 and 25 by the apparent rate constant, which mathematical expression was presented in Eq. 27.

$$k_{2,app} = \frac{k_2[H^+]^2 + k_3 K_A [H^+]}{\left(K_A + [H^+]\right)\left(K_B + [H^+]\right)} \quad (27)$$

Where here k_2 and k_3 are the true rate constants of the reactions R6 and R7 respectively and K_A and K_B are the acid-base equilibrium constants for the ACE ($K_A = 10^{-9.7}$) [22] and the HOCl ($K_B = 10^{-7.53}$) [19, 21] respectively. The solution of Eq. 26 provides the OH^- concentration and then the H^+ concentration for Eq. 27. Thus, Eqs. 23-27 provide the numerical model used in this work to represent the experimental observations.

Once obtained the experimental data, the model should be validated after a non-linear least-squares fitting procedure matching the experiments with the model [24]. Related to this procedure, it was relevant to the analysis of the sensitivity of the model, i.e., the relative effect of the parameters defined in the model over each observable magnitude. The sensitivity matrix was related to the Jacobian

matrix of the Eqs. 23-27, using matrix notation, the relative sensitivity matrix, S(t,p) is defined by Eq. 28.

$$\mathbf{S}(t,\mathbf{p}) = \mathbf{p}\frac{\partial \mathbf{q}(t,\mathbf{p})}{\partial \mathbf{p}} \tag{28}$$

Where p is the vector of parameters and q is the vector of state variables (Eqs. 29 and 30) in the model.

$$\mathbf{p} = \begin{pmatrix} \Phi_E & k_1 & k_2 & k_3 & \tau_H & C_{A0} & C_{OH}^0 & \frac{1}{\eta} - 1 \end{pmatrix}^T \tag{29}$$

$$\mathbf{q} = \begin{pmatrix} z & x & y & w \end{pmatrix}^T \tag{30}$$

Because the model represented by Eqs 23-27 has no analytic, nor explicit solution, is not possible the direct evaluation of the sensitivity matrix (Eq. 28). Instead, this direct evaluation, it is possible to define a new set of ODEs (Eq. 31) related to the time-derivative of the sensitivity:

$$\frac{d\mathbf{S}(t,\mathbf{p})}{dt} = \mathbf{p}\frac{\partial}{\partial \mathbf{p}}\left(\frac{d\mathbf{q}(t,\mathbf{p})}{dt}\right) = \mathbf{p}\frac{\partial \dot{\mathbf{q}}}{\partial \mathbf{p}} \tag{31}$$

This last set of differential equations was solved together with Eqs. 23-27, defining the group. Because the group is considered at rest with t = 0, i.e. the system initially is under a steady-state, the initial condition of Eq. 31 is S(0, p) = 0.

To evaluate the relevance of each parameter of the model (Eq. 29) on each state variable (Eq. 30), we need some metric which integrates the relative sensitivity of the model along with all the responses of the system. For this purpose, we propose the integrated relative sensitivity parameter, σ_{ij} (Eq. 30).

$$\sigma_{ij}^2 = \int_0^\infty \left[p_j \left(\frac{\partial q_i}{\partial p_j} \right) \right]^2 dt \quad (32)$$

Because the asymptotic solution of Eqs 23-27 gives a steady-state concentration with all the state variables constant, the solution of Eq. 31; i.e., S(t, p), must be a bounded function and then, the Eq. 32 is a convergent and a positive magnitude. This metric is a matrix that gives the relative importance of each parameter of the model on each state variable. Once this matrix is normalized with its maximum value, with the value of σ_{ij} is possible to sort the relative importance of each of the parameters for each state variable.

The relative sensitivity of the parameters is a local analysis that depends on the set point in the space parameters where the analysis is done. Then the results depend on the specific values for the parameters. This analysis provides relevant information to calculate accurately the parameters from experimental data.

3. Results and discussions

3.1. Ability of the electrochemical system to generate RCS

The effect of two main operational parameters (I and Q) on the production of RCS by the considered reaction system was evaluated through an experimental design (Table S1) in absence of pharmaceuticals. Fig. 1**¡Error! No se encuentra el origen de la referencia.** shows the response surface for the accumulation of RCS upon the variation of both I and Q in the considered electrochemical reactor.

From Fig. 1, it can be noted the trends for each parameter, and the red zone indicates the most suitable values of the current and flow parameters for the RCS production. The trends showed that the increase in the current intensity favors the RCS formation, which is associated with the improvement of electronic transfer between the chloride anions and DSA surface (R1, Table 1) as the current is augmented [25]. Conversely, a lower value of the flow increases the contact time of the electrolyte (chlorine ions) on the surface of the DSA and so enhances the formation of RCS [16, 26]. Thereby, in considered ranges, the highest value of I and the lowest amount of Q (which corresponded to 100 mA and 11 mL min^{-1}, respectively) were the most suitable conditions for the RCS generation in the tested electrochemical system.

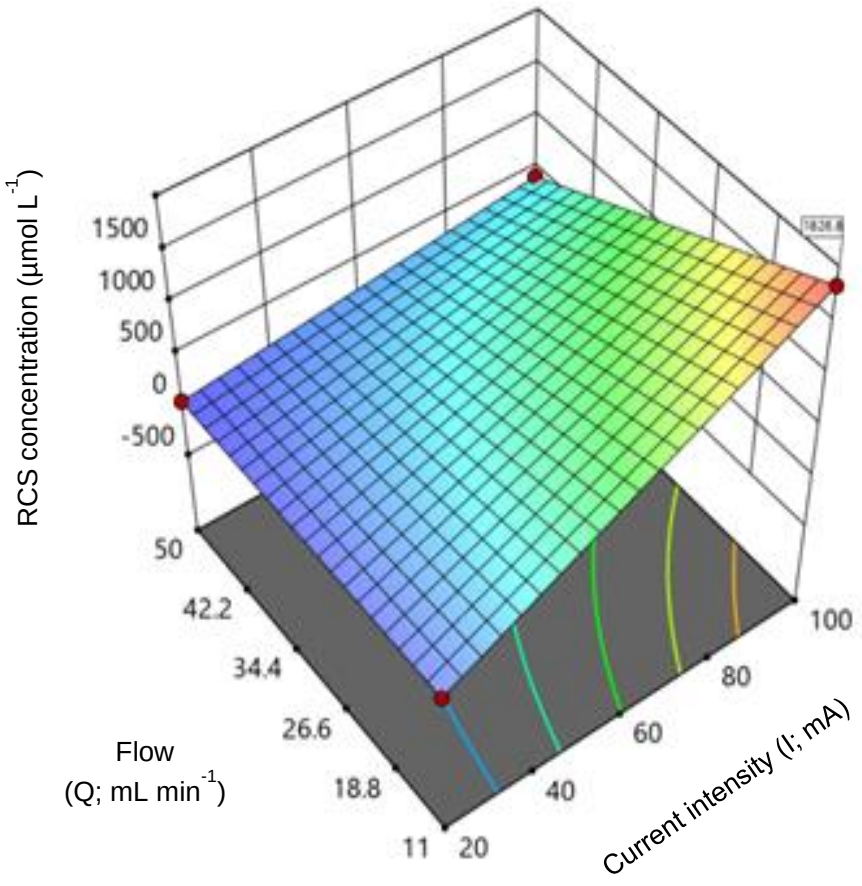

Fig 1. Response surface derived from the DOE for the effect of current intensity and flow. Operational conditions: current intensity (I) = 20 to100 mA, flow (Q)= 11 to 50 mL min^{-1}, with 0.1 mol L^{-1} of NaCl.

3.2. Degradation of ACE in the electrochemical system under favorable conditions

After determining the proper conditions of I and Q for the RCS production, the action of the electrochemical system, under such conditions, on the pharmaceutical ACE was evaluated. The ACE removal percentage at 10 min of treatment is

shown in Fig. 2. In addition to the ACE degradation, the accumulations of RCS in the presence and absence of ACE were measured and compared (Fig. 2).

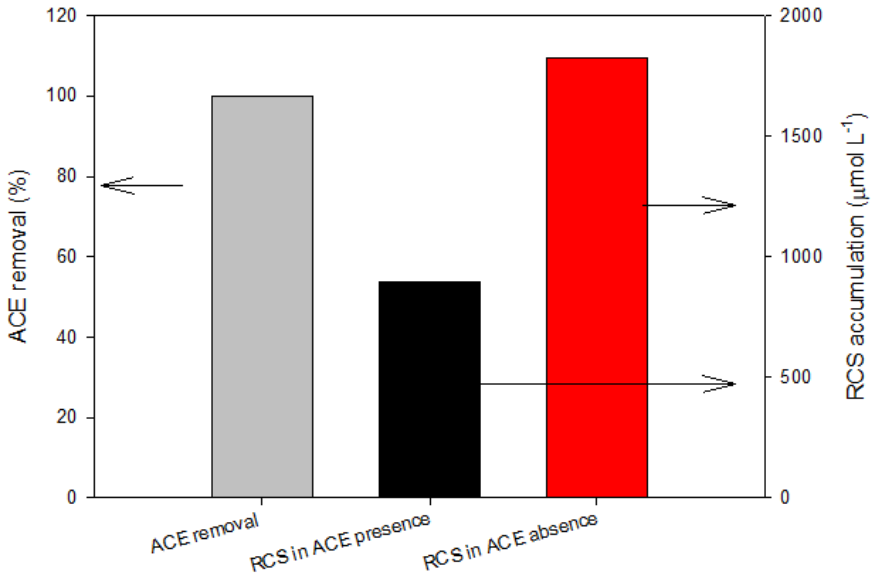

Fig. 2. ACE removal, and RCS accumulation in presence and absence of ACE after 10 min of treatment in distilled water. Experimental conditions: [ACE] = 40 mg L^{-1}, I = 100 mA, Q= 11 mL min^{-1}, and [NaCl]= 0.1 mol L^{-1}.

The electrochemical system induced a high removal of ACE (~100% at 10 min of treatment) and the RCS accumulation is lower in the pharmaceutical presence than in its absence (Fig. 2). These results indicate that the electrogenerated RCS effectively degrades ACE. Due to the reaction between ACE and the electrogenerated species, the RCS accumulation was diminished a half approximately. As mentioned above, the RCS are powerful oxidizing agents able to attack organic

compounds such as ACE [23]. In fact, RCS can chlorinate ACE, producing compounds such as 1,4-benzoquinone, *N*-acetyl-*p*-benzoquinone imine (NAPQI), and intermediaries from chlorination on the aromatic ring [21,27,28].

Despite the treatment of ACE by electrogenerated RCS or conventional chlorination has been widely considered in the literature [21,27–29], few works have been addressed to the modeling of its degradation by these species. Therefore, the topic of modeling was studied as discussed, as detailed in the following section.

3.3. Modeling of the ACE degradation and RCS production

In the initial part of the modeling, the chlorine evolution at different current intensities (Fig. 3A) and concentration of supporting electrolyte (Fig. 3B), both in presence of ACE, has been estimated using Eqs. 23-27. In Fig. 3, the line represents the values obtained by modeling and the dots correspond to the experimental results.

The results show that the RCS accumulation is higher when increasing the applied current in the electrochemical cell (Fig. 3A). As above mentioned, as the current is augmented the electronic transfer between the chloride anions DSA surface is increased. Moreover, the RCS rate formation also increases as the chloride ion concentration was higher (Fig. 3B). This behavior is associated with the enhancement of the conductivity of the solution and mass transference of

chloride ions toward the anode surface [25]. Interestingly, the modeling lines represent well the trends of the experimental points and the variation of I and Cl^- concentration. This is consistent with the HOCl concentration dependence on Φ_E (as indicated in Eq. 17), which is directly linked with the current intensity and the concentration as will be demonstrated below.

A

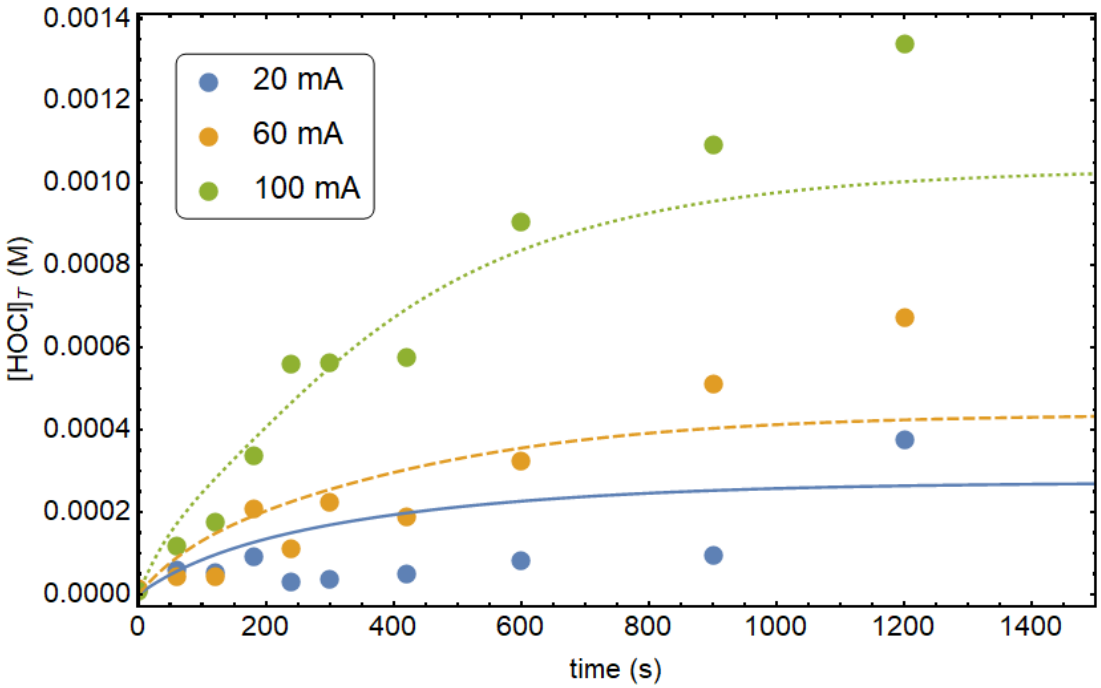

B

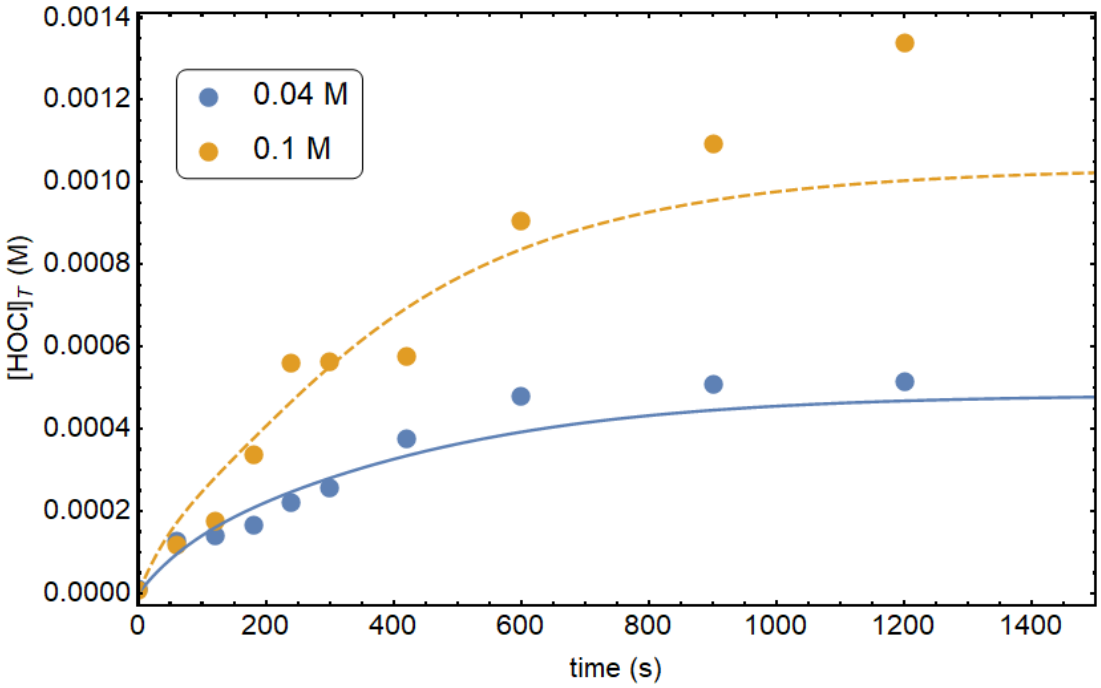

Fig. 3. HOCl evolution. **A.** Dependence on the applied current (I= 20, 60 and 100 mA) at [NaCl] = 0.1 mol L^{-1}; Q = 11 mL min^{-1}, and ACE = 40 mg L^{-1}. **B.** Dependence on NaCl concentrations ([NaCl]= 0.04 and 0.1 mol L^{-1}; at I = 100 mA; Q= 11 mL min^{-1}, and ACE = 40 mg L^{-1}). The experimental data are the dots and the modeled results are shown as lines.

Once the RCS evolution was modeled, the parameter Φ_E was calculated**¡Error! No se encuentra el origen de la referencia.**. Fig. 4 shows that under the experimental conditions, Φ_E has a linear direct dependence on I and Cl^- concentration. Consequently, the chlorine rate formation can be expressed as a mathematical function of both current and chloride anion concentration as presented in Eq. 33.

$$\Phi_E(M/s) = 4.34 \cdot 10^{-4}\ (A^{-1}\ s^{-1}) \cdot I \cdot [Cl^-] \qquad (33)$$

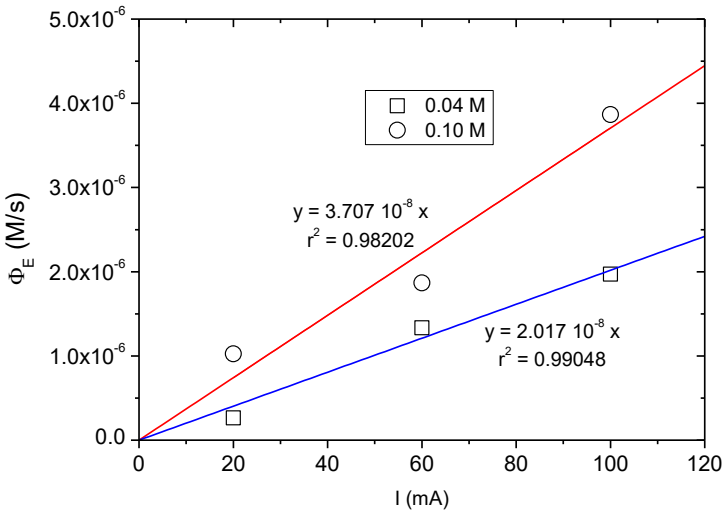

Fig. 4. RCS rate production (Φ_E) from the model and the experimental results as a function of the applied current intensity and supporting electrolyte (NaCl) concentration.

After the determination of Φ_E, the pH variation at the output of the reactor was also modeled, as shown in **¡Error! No se encuentra el origen de la referencia.**. It can be noted that the pH raises to high values in short times and reaches its steady-state which can be evaluated through Eq. 34 (which was obtained from Eq. 26). The increase of pH can be explained by considering the reduction of water on the cathode (R8 in Table 1). Due to a part of the electrogenerated acid species (i.e., HOCl) was consumed by ACE degradation, hydroxide anions were accumulated increasing fastly the pH up to achieve a plateau. It can be noted that the model (solid lines in Fig. 5) represents approximately well the effect of current

on the pH variation, especially between 0 and 420 s of electrolysis. At long treatment times (i.e., > 420 s), a decrease in the experimental data for pH was observed, which suggests that the primary byproducts coming from the ACE degradation do not consume RCS significantly, and acid species such as HOCl can react with the OH^-, thus diminishing the pH. These last aspects were not considered in Eq. 34, and this explains the differences between the experimental data and the values obtained using the model.

$$pH^{SS} = pH_0 + \log\left(1 + \frac{\Phi_E \, \tau_H}{C_{OH}^0}\left(\frac{1}{\eta} - 1\right)\right) \tag{34}$$

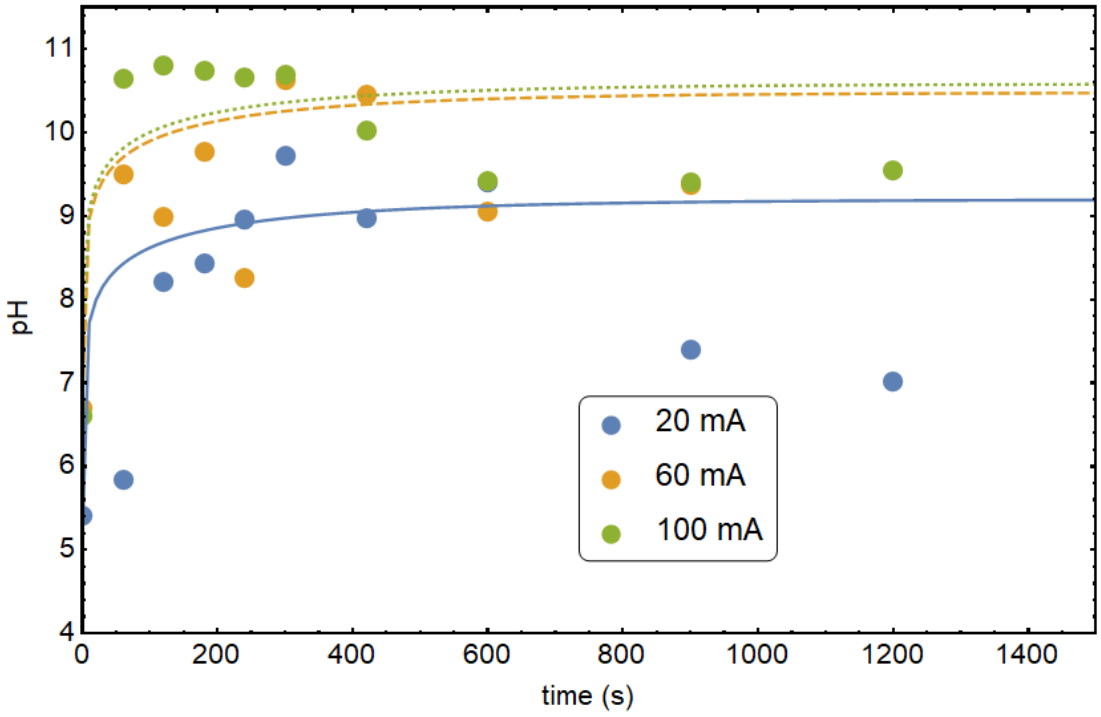

Fig. 5. pH profiles at the output of the electrochemical reactor in presence of ACE for different applied currents I= 20, 60, and 100 mA. Experimental conditions:

[NaCl] = 0.1 mol L^{-1}; Q= 11 mL min^{-1}, and [ACE]= 40 mg L^{-1}. The experimental data (circles) are shown for different initial concentrations.

In addition to the evolution of RCS and pH, the degradation of ACE, at different initial concentrations, was also modeled. Fig. 6**¡Error! No se encuentra el origen de la referencia.** shows that for initial concentrations concentration between 10 and 40 mg L^{-1} of ACE, the electrochemical system completely degraded the pharmaceutical. Indeed, at 60 mg L^{-1} of ACE, the pollutant degradation achieved a steady-state, indicating that this system had a maximum removal capability of ~ 40 mg L^{-1} of the initial amount under the tested conditions. Furthermore, from Fig. 6, it can be noted that the values from the model fit quite well to the experimental observations for all the ACE concentrations. This proves that the model based on the intrinsic parameters or the reactor (i.e., $\tau_{H,}$ and Φ_E), and interaction between the pharmaceutical and RCS (e.g., $k_{2,\,app}$) represents the ACE degradation by the system correctly. Moreover, our results are in good agreement with previous works that also report the dependence of ACE degradation on concentrations of the pollutant and RCS [27], and the strong influence of current and supporting electrolyte (which control Φ_E) [29], in addition to the pH and contact time [27,28].

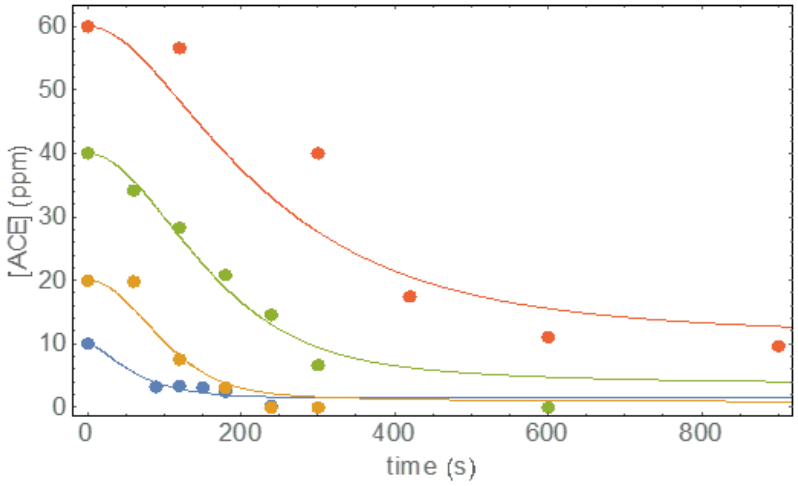

Fig. 6. ACE profiles at the output of the electrochemical reactor. The experimental data are shown in circles, whereas the model is represented by the solid lines. Experimental conditions: [ACE] = 10, 20, 40 and 60 ppm (mg L^{-1}); [NaCl]= 0.1 mol L^{-1}; Q= 11 mL min^{-1}, I= 100 mA, $pH_{initial}$ = 6.0.

On the other hand, in the modeling of processes, sensitivity analyses are relevant to determine the relative importance of each parameter regarding both the mathematical structure of the model and the experimental data [30]. Thereby, the sensitivity analysis of our model was performed for the neighborhood of a given set point of the model. We used the parameters in Table 2 as the operational set point, which reproduces the experimental observations. In the calculations, we used Eq. 31. This equation relates the sensitivity, S(t), with the state variables, q(t), of the model. In turn, the state variables are related to the observables, which are the concentrations that we can measure at the output of the reactor. Then,

we have the observation matrix C(p) that relates the observables with the state variables, according to Eq. 35.

$$\mathbf{y}(t,\mathbf{p}) = \mathbf{C}(\mathbf{p}) \cdot \mathbf{q}(t,\mathbf{p}) \tag{35}$$

Where p is the parameter vector of the model (see Ec. 29). For our system, Ec. 35 took the explicit form presented in Eq. 36.

$$\begin{pmatrix} C_{Cl_2} \\ C_{HOCl} \\ C_{ACE} \\ C_{OH} \end{pmatrix} = \begin{pmatrix} \frac{\Phi_E}{k'} & 0 & 0 & 0 \\ 0 & \frac{\Phi_E\ \tau_H\ k_1}{k'} & 0 & 0 \\ 0 & 0 & C^0_{ACE} & 0 \\ 0 & 0 & 0 & C^0_{OH} \end{pmatrix} \begin{pmatrix} z \\ x \\ y \\ w \end{pmatrix} \tag{36}$$

The combination of Eqs. 31 and 35 produced the observable system represented by Eq. 37.

$$\frac{d\mathbf{S}_\mathbf{y}}{dt} = \mathbf{p}\left[\mathbf{C}\frac{\partial \dot{\mathbf{q}}}{\partial \mathbf{p}} + \dot{\mathbf{q}}\frac{\partial \mathbf{C}}{\partial \mathbf{p}}\right] = \mathbf{p}\frac{\partial \dot{\mathbf{y}}}{\partial \mathbf{p}} \tag{37}$$

Solving the system of ordinary differential equations presented by Eq. 37 with Sy(0) = 0 together Eqs. 23-27, we calculated the matrix presented in Eq. 32. Using the parameters of Table 2, the relative sensitivity matrix (Eq. 32) had the following explicit form.

$$\begin{pmatrix} 1.64\cdot10^{-4} & 1.64\cdot10^{-4} & 0 & 0 & 2.43\cdot10^{-8} & 0 & 0 & 0 \\ 0.9981 & 5.36\cdot10^{-4} & 5.75\cdot10^{-8} & 3.81\cdot10^{-4} & 0.8916 & 3.02\cdot10^{-4} & 0 & 0 \\ 7.62\cdot10^{-4} & 3.81\cdot10^{-4} & 5.75\cdot10^{-8} & 3.81\cdot10^{-4} & 6.66\cdot10^{-4} & 0.2348 & 0 & 0 \\ 1.16\cdot10^{-3} & 1.64\cdot10^{-4} & 0 & 0 & 8.93\cdot10^{-4} & 0 & 2.80\cdot10^{-5} & 1.0 \end{pmatrix}$$

(38)

This last matrix was translated into a heat map, where the color intensity is related to the value of each element, resulting in Fig. 7. In Fig. 7, columns correspond to the parameters of the model given by Eq. 29 and the rows correspond to each observable variable, namely the concentrations of Cl_2, HOCl, ACE, and OH^-.

Table 2. Reference values for the determination of the sensitivity analysis.

Symbol	Value*	Units
Φ_E	3.444 x 10^{-6}	M s^{-1}
k_1	20.9[(a)]	s^{-1}
k_2	3.1[(b)]	M^{-1} s^{-1}
k_3	7000[(b)]	M^{-1} s^{-1}
τ_H	329.3	s
C^0_{ACE}	2.64 x 10^{-4}	M
C^0_{OH}	$10^{-7.5}$	M
η	0.999	-

*The values are close to the mean experimental values. [(a)] Spalding et al. [31], [(b)] Pinkston et al. [21]. -:Dimensionless.

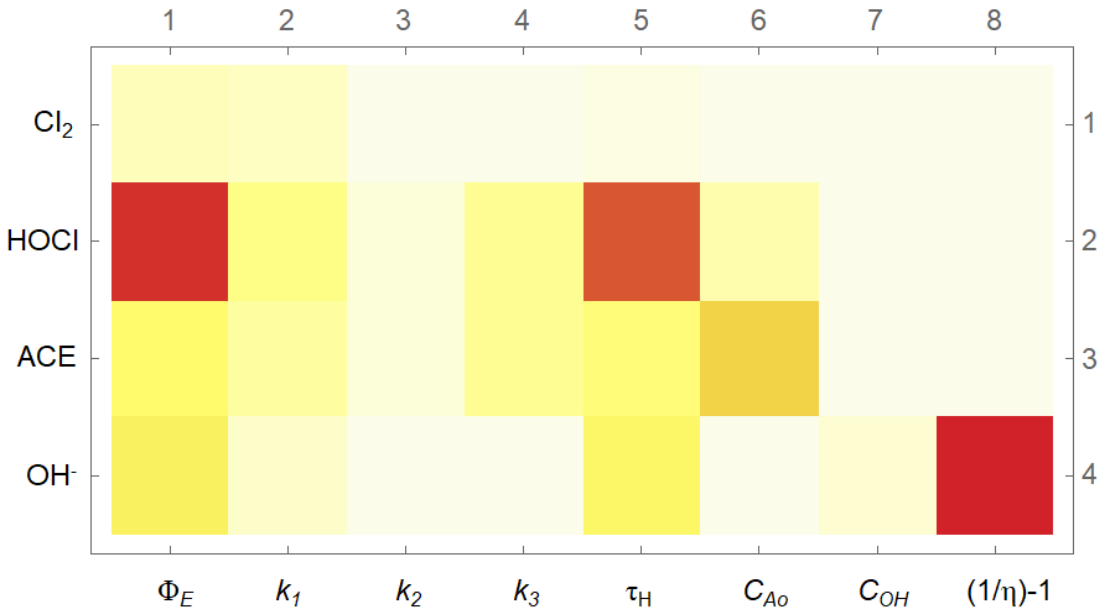

Fig. 7. Results of the sensitivity analysis for the model. The columns are the model parameters and the rows correspond to each observable variable.

From Fig. 7, we can remark that the most relevant parameters of the model were Φ_E and τ_H for the accumulation of HOCl, and the η parameter for the production of OH^-. The results about the accumulation of HOCl agree with the findings informed by other authors about modeling of heterogeneous generation of RCS in an analogous electrochemical system. They also found that the inlet flow (parameter related to τ_H) and the current (parameter linked to Φ_E) are very important for the accumulation of RCS [16].

Regarding the ACE degradation, the parameters C^0_{ACE}, Φ_E, and τ_H were relevant but the kinetic constants had a lower influence on the ACE response. Thereby, these results from the sensitivity analysis indicated that for the considered system,

the reactor operational parameters had a higher influence on the response than the reaction rate constants.

3.4. Application of the electrochemical treatment to degrade pharmaceuticals in seawater

Once considered the degradation of ACE by the electrogenerated RCS in distilled water, the feasibility of the electrochemical process to eliminate this pharmaceutical in an aqueous complex matrix (actual seawater from the Pacific Ocean, Table 3) was evaluated, and subsequently simulated. We evaluated the treatment of ACE (at 5.0 mg L^{-1}) in actual seawater. In this case, a non-negligible organic matter in seawater able to react with the RCS has been considered. This means that together the chemical reaction R3-R7 in Table 1, it should be included the chemical reaction between the RCS and the natural organic matter, represented as B in Eq. 39.

$$HOCl + B \xrightarrow{k_B} Prods \tag{39}$$

Under these circumstances, Eq. (24) changes to Eq. 40.

$$\frac{dx}{dt} = \tau_H^{-1}(z - x) - C_{A0}\, k_2\, x\, y_A - C_{B0}\, k_B\, x\, y_B \tag{40}$$

The dimensionless concentration of the ACE has been written as y_A here, and y_B is the dimensionless organic matter concentration defined as $y = {C_B}/{C_{B0}}$.

Additionaly, a new differential equation must be added to the system of Eqs. 23-26 accounting for the oxidation of natural organica matter. Similar to Eq. 25, the mass balance of the reactive natural organic matter gives Eq. 41.

$$\frac{dy_B}{dt} = \tau_H^{-1}(1 - y_B) - \tau_H \, \Phi_E \, k_B \, x \, y_B \tag{41}$$

Where k_B is the reaction rate constant for the reaction between the RCS and the organic matter present in the seawater wich in order of simplicity, has been considered independent of the pH.

Table 3. Main characteristics of the actual seawater.

Substances/parameter	Units	Value
Cl^-	mol L^{-1}	0.55
Br^-	mmol L^{-1}	0.69
F^-	mmol L^{-1}	0.07
SO_4^{2-}	mol L^{-1}	0.03
HCO_3^-	mmol L^{-1}	2.15
Na^+	mol L^{-1}	0.43
K^+	mol L^{-1}	0.01
Mg^{2+}	mol L^{-1}	0.03
Ca^{2+}	mol L^{-1}	0.01
pH	-	6.4
Conductivity	mS cm^{-1}	47.9
Total organic carbon	mg L^{-1}	3.2

A

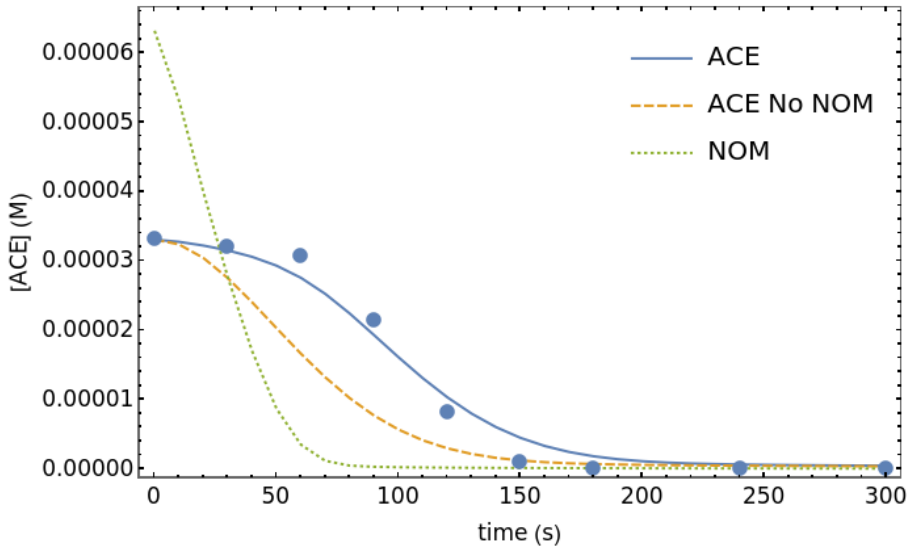
ACE
ACE No NOM
NOM
[ACE] (M)
0.00006
0.00005
0.00004
0.00003
0.00002
0.00001
0.00000
0
50
100
150
200
250
300
time (s)

B

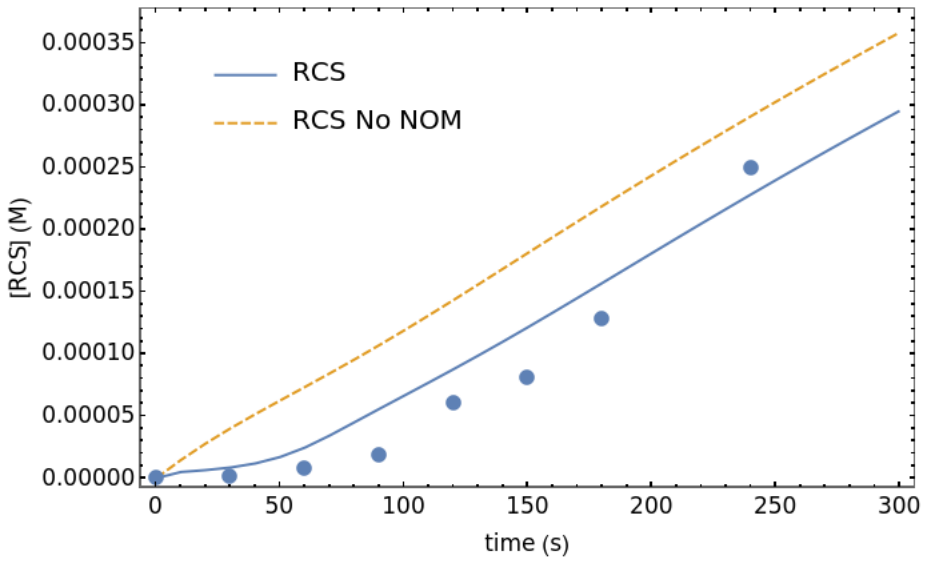
RCS
RCS No NOM
[RCS] (M)
0.00035
0.00030
0.00025
0.00020
0.00015
0.00010
0.00005
0.00000
0
50
100
150
200
250
300
time (s)

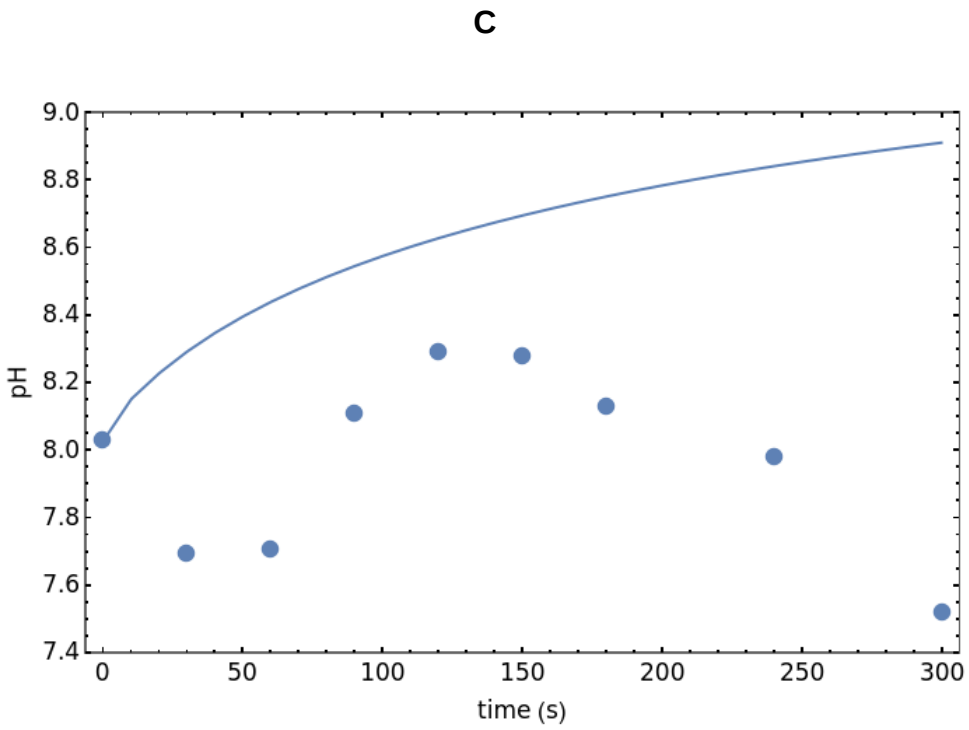

Fig. 8. Treatment of ACE in real seawater by the electrochemical system. **A.** Degradation of ACE. **B.** Evolution of RCS during degradation of ACE in seawater. **C.** pH evolution during degradation of ACE in seawater. Blue dots: experimental data, blue line: simulated values in the NOM presence, orange dashed line: simulated values in the NOM absence, green dashed line: simulated values for NOM oxidation. Experimental conditions: [ACE]= 5 mg L^{-1} (33.1 µmol L^{-1}), I= 100 mA, and Q= 11 mL min^{-1}.

The dots in Fig. 8A depicts the evolution of ACE in the actual seawater. It can be noted that the electrochemical system was able to completely degrade ACE after 180 s of treatment. This fast ACE degradation can be associated with the high amount of RCS produced from the intrinsic chloride ions (0.55 mol L^{-1}, Table 3)

in the seawater, which favors the charges conduction and the production of the degrading species [25].

Despite the fast degradation of the analgesic in the actual seawater, we should mention that in distilled water (containing 0.5 mol L^{-1} of NaCl), ACE was degraded after only 30 s of electrolysis (Fig. S3). This fact can be explained by considering the composition of real seawater. The actual matrix is rich in inorganic ions (e.g., chloride) that are useful for the development of the electrochemical process. Nonetheless, at the same time, the seawater also has natural organic matter (i.e., 3.2 mg L^{-1} of total organic carbon, Table 3) that can react with the electrogenerated RCS [16], slowing the ACE removal regarding the distilled water.

Fig. 8A also shows the corresponding simulations for ACE degradation in seawater considering the absence (orange dashed line) and presence (blue line) of intrinsic natural organic matter (NOM) in this matrix. Additionally, the evolution of the oxidation of the NOM has been represented in Fig. 8A. As expected, a shift in the ACE curve at higher treatment times occurred when the NOM is taken into account. Moreover, the RCS can attack NOM, leading to its degradation, as illustrated by the green dashed line in Fig. 8A. It should be noted that the concentration of NOM is around twice the concentration of ACE, and the simulation suggested that the reaction rate of NOM with RCS is significantly higher than the reaction rate between ACE and RCS.

In addition to the ACE degradation, during the treatment of this pharmaceutical in the seawater matrix, the evolution of the RCS and pH were followed and simulated. The simulation of the chlorine species evolution (Fig. 8B) showed that the presence of NOM diminishes the concentration of RCS concerning its absence, which is consistent with the results presented in Fig. 8A. Thus, the proposed approach with the model proposed in this work was successful in reproducing the observations about ACE degradation and RCS evolution in actual seawater.

Regarding the pH behavior, the simulation did not represent well the results in the seawater matrix (Fig. 8C), which demonstrates the high difficulty for the modeling of this parameter. From the experimental data in Fig. 8C (i.e., the blue dots), it can be noted that during the ACE treatment in the seawater, the pH oscillated a little around 8.0, contrasting with the higher pH variations observed in distilled water (Fig. 5). Such differences suggest seawater had a certain buffering capacity (due to the presence of anion bicarbonate, Table 3), which was not observed in distilled water. Moreover, the buffering ability of the actual matrix was not included in the pH model, and therefore, the simulated values of pH were above the experimental ones (Fig. 8C).

On the other hand, to assess the degrading ability of the electrochemical system on other pharmaceuticals, the treatment in seawater of the highly consumed antibiotic ciprofloxacin (CIP, at ~11 mg L^{-1}, which corresponded to the same molar

concentration used for ACE) was considered. Furthermore, to determine the electrochemical treatment extent, the removal of the antimicrobial activity (AA) associated with the antibiotic was also measured. Fig. 9A compares the evolutions of CIP and ACE during their treatment in seawater, whereas Fig. 9B and AA under the electrochemical treatment, respectively.

The comparison between the treatment of the two pharmaceuticals shows that the degradation of the antibiotic CIP was faster than the analgesic ACE (Fig. 9A). This difference can be related to the chemical structural properties of each pharmaceutical (Fig. S4), which determine their interactions with the RCS [23,32]. CIP has two amines on the piperazinyl ring, which are very reactive toward the chlorine species, and this ring can be opened by HOCl (Fig. S4A) [33,34]. Furthermore, in the CIP structure, the benzene carbon placed in ortho position to the piperazinyl moiety and meta position to the fluorine atom is activated, and then undergoes an electrophilic aromatic substitution promoted by chlorine species (see Fig. S4B) [33]. Meanwhile, the ACE structure contains a phenol moiety and an acetamide group. These two groups are susceptible to chlorination (as illustrated in Fig. S4C-D) [29]. Nevertheless, phenol and acetamide on ACE are less reactive than amines (as those present in CIP) toward RCS. Indeed, the second-order reaction rate constant between RCS and CIP (k: 3.8 x10^5 M^{-1} s^{-1}) is higher than that for ACE (k: 3.1 M^{-1} s^{-1}) [23], thus explaining the faster elimination of the antibiotic by the system.

A

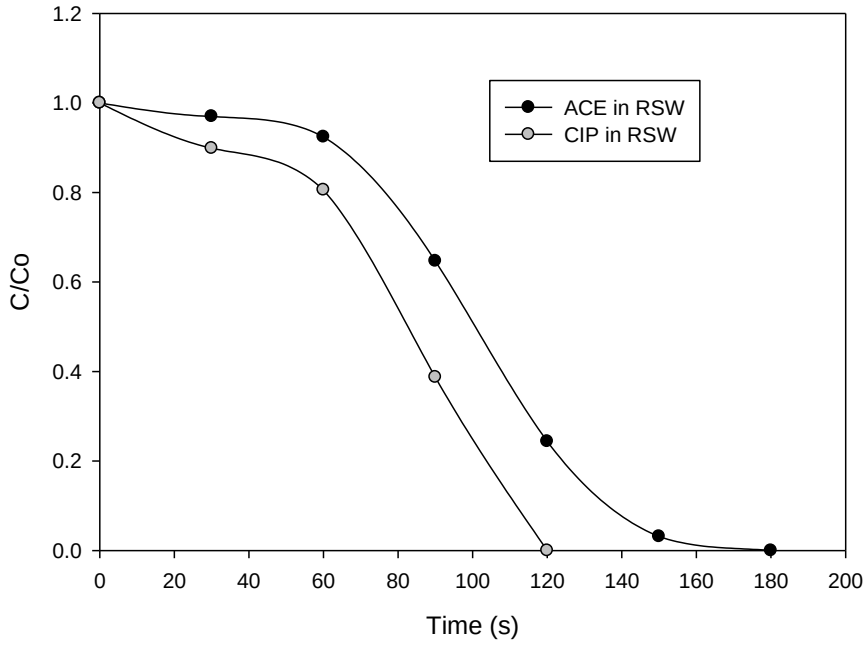
ACE in RSW
CIP in RSW
C/Co
Time (s)
0.0
0.2
0.4
0.6
0.8
1.0
1.2
0
20
40
60
80
100
120
140
160
180
200

B

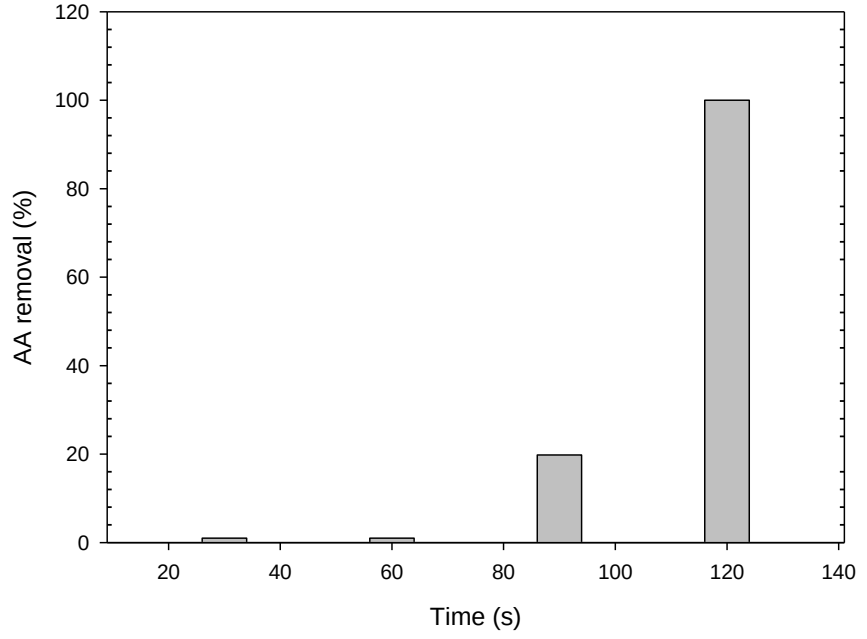
AA removal (%)
Time (s)
0
20
40
60
80
100
120
20
40
60
80
100
120
140

Fig. 9. Treatment of pharmaceuticals in real seawater by the electrochemical system. **A.** comparison of ACE and CIP degradation in real seawater (RSW). **B.** removal of the antimicrobial activity AA associated with the antibiotic CIP. Experimental conditions: [ACE]= [CIP]= 33.1 μmol L^{-1}, I= 100 mA. Pharmaceuticals were treated individually. *S. aureus* was used as the indicator microorganism for AA.

Regarding the AA (Fig. 9B), it can be noted that the process eliminated the activity after only 120 s of treatment (when more than 98% of CIP was degraded). As mentioned above, the electrogenerated RCS are able to attack the piperazinyl moiety and transform the aromatic ring on CIP (Fig. S4A-B). The piperazyl ring controls the antimicrobial potency and pharmacokinetic properties of fluoroquinolone antibiotics like CIP [35,36], and the chlorination of the benzene ring can alter the activity against bacteria [37]. Then, the structural modifications may be responsible for the AA removal. Moreover, the AA elimination represented a positive aspect for the electrochemical treatment of pharmaceuticals in complex aqueous samples (like seawater) because AA removal can contribute to the decrease of adverse effects of the input of antibiotics into the environment.

4. Conclusions

From the development of the present research, it was concluded that for the considered electrochemical system (a filter-press reactor, equipped with a dimensionally stable anode, NaCl, and operated in continuous mode), high current and low flow were convenient for the RCS production through the enhancement of electronic transfer and the contact time between the chloride anions and DSA surface. The semi-empirical model based on CSTR hypothesis and the definition of the RCS rate production was proposed and successfully applied to account for the production of RCS, ACE degradation at different concentrations, and pH evolution. The developed model allowed us to establish a mathematical relationship among the RCS generation, current intensity, and chloride anions concentration. Moreover, the ACE degradation by the electrochemical system was correctly represented by the model due to this involved both the reactor (i.e., $\tau_{H,}$ and Φ_E) and interaction between the pharmaceutical and RCS (e.g., $k_{2,\,app}$). The relevance of $\tau_{H,}$ and Φ_E in addition to the pharmaceutical concentration, in the ACE degradation, was confirmed the sensitivity analysis. The electrochemical process was able to fastly remove ACE in the actual seawater. Furthermore, the analgesic degradation and RCS evolution were properly simulated considering in the model the reaction of chlorine species with the intrinsic NOM present in the actual matrix. On the other hand, the electrochemical system also degraded CIP in the real seawater and eliminated its related AA (which was associated with structural transformations of the antibiotic), and this removal denotes a positive action of the

system to decrease the environmental impacts of CIP. Finally, we can suggest that the results from the kinetic modeling of ACE degradation could be utilized in further works as a background to study fundamental and practical aspects of degradation of other pharmaceuticals in water by electrogenerated RCS.

Acknowledgments

The authors from GICAB acknowledge the financial support provided by Fondecyt/Concytec-Perú through the project CP-8682-PE-BM-Fondecyt/Concytec (Cont. 032-2018-Fondecyt-BM-IADT-AV). The authors from GIRAB acknowledge the support provided by Universidad de Antioquia UdeA by means "*Programa de Sostenibilidad*". E. A. Serna-Galvis thanks MINCIENCIAS COLOMBIA for his Ph.D. fellowship during July 2015-June 2019 (Convocation 647 de 2014), and the Postdoctoral scholarship (Convocation 848-2019).

References

[1] K. Nödler, D. Voutsa, T. Licha, Polar organic micropollutants in the coastal environment of different marine systems, Mar. Pollut. Bull. 85 (2014) 50–59. https://doi.org/10.1016/j.marpolbul.2014.06.024.

[2] P. Sathishkumar, R.A.A. Meena, T. Palanisami, V. Ashokkumar, T. Palvannan, F.L. Gu, Occurrence, interactive effects and ecological risk of diclofenac in environmental compartments and biota - a review, Sci. Total

Environ. 698 (2020) 134057. https://doi.org/10.1016/j.scitotenv.2019.134057.

[3] J. Du, H. Zhao, Y. Wang, H. Xie, M. Zhu, J. Chen, Ecotoxicology and Environmental Safety Presence and environmental risk assessment of selected antibiotics in coastal water adjacent to mariculture areas in the Bohai Sea, Ecotoxicol. Environ. Saf. 177 (2019) 117–123. https://doi.org/10.1016/j.ecoenv.2019.03.075.

[4] V. Homem, L. Santos, Degradation and removal methods of antibiotics from aqueous matrices – A review, J. Environ. Manage. 92 (2011) 2304–2347. https://doi.org/10.1016/j.jenvman.2011.05.023.

[5] I.T. Carvalho, L. Santos, Antibiotics in the aquatic environments: A review of the European scenario, Environ. Int. 94 (2016) 736–757. https://doi.org/10.1016/j.envint.2016.06.025.

[6] H. Montaseri, P.B.C. Forbes, Analytical techniques for the determination of acetaminophen: A review, TrAC - Trends Anal. Chem. 108 (2018) 122–134. https://doi.org/10.1016/j.trac.2018.08.023.

[7] C. Ng, S.G. Goh, N. Saeidi, W.A. Gerhard, C.K. Gunsch, K.Y.H. Gin, Occurrence of Vibrio species, beta-lactam resistant Vibrio species, and indicator bacteria in ballast and port waters of a tropical harbor, Sci. Total Environ. 610–611 (2018) 651–656. https://doi.org/10.1016/j.scitotenv.2017.08.099.

[8] R.R. Redfield, Antibiotic resistance threats in the United States, Centers Dis. Control Prev. (2019) 148. https://doi.org/CS239559-B.

[9] I. Michael, L. Rizzo, C.S. McArdell, C.M. Manaia, C. Merlin, T. Schwartz, C. Dagot, D. Fatta-Kassinos, Urban wastewater treatment plants as hotspots for the release of antibiotics in the environment: A review, Water Res. 47 (2013) 957–995. https://doi.org/10.1016/j.watres.2012.11.027.

[10] M.Á. López Zavala, D.A. Vega, J.M. Álvarez Vega, O.F. Castillo Jerez, R.A. Cantú Hernández, Electrochemical oxidation of acetaminophen and its transformation products in surface water: effect of pH and current density, Heliyon. 6 (2020). https://doi.org/10.1016/j.heliyon.2020.e03394.

[11] R.E. Palma-Goyes, J. Vazquez-Arenas, C. Ostos, F. Ferraro, R.A. Torres-Palma, I. Gonzalez, Microstructural and electrochemical analysis of Sb2O5 doped-Ti/RuO2-ZrO2 to yield active chlorine species for ciprofloxacin degradation, Electrochim. Acta. 213 (2016) 740–751. https://doi.org/10.1016/j.electacta.2016.07.150.

[12] C.A. Martínez-Huitle, E. Brillas, Decontamination of wastewaters containing synthetic organic dyes by electrochemical methods: A general review, Appl. Catal. B Environ. 87 (2009) 105–145. https://doi.org/10.1016/j.apcatb.2008.09.017.

[13] I. Sirés, E. Brillas, Remediation of water pollution caused by pharmaceutical residues based on electrochemical separation and

degradation technologies : A review, Environ. Int. 40 (2012) 212–229. https://doi.org/10.1016/j.envint.2011.07.012.

[14] E.P. Rivero, F.F. Rivera, M.R. Cruz-Díaz, E. Mayen, I. González, Numerical simulation of mass transport in a filter press type electrochemical reactor FM01-LC: Comparison of predicted and experimental mass transfer coefficient, Chem. Eng. Res. Des. 90 (2012) 1969–1978. https://doi.org/10.1016/j.cherd.2012.04.010.

[15] M.R. Cruz-Díaz, E.P. Rivero, F.J. Almazán-Ruiz, Á. Torres-Mendoza, I. González, Design of a new FM01-LC reactor in parallel plate configuration using numerical simulation and experimental validation with residence time distribution (RTD), Chem. Eng. Process. Process Intensif. 85 (2014) 145–154. https://doi.org/10.1016/j.cep.2014.07.010.

[16] R.E. Palma-Goyes, F.F. Rivera, J. Vazquez-Arenas, Heterogeneous Model to Distinguish the Activity of Electrogenerated Chlorine Species from Soluble Chlorine in an Electrochemical Reactor, Ind. Eng. Chem. Res. 58 (2019) 22399–22407. https://doi.org/10.1021/acs.iecr.9b05185.

[17] R.E. Palma-Goyes, J. Vazquez-Arenas, C. Ostos, A. Manzo-Robledo, I. Romero-Ibarra, J.A. Calderón, I. González, In search of the active chlorine species on Ti/ZrO2-RuO2-Sb2O3 anodes using DEMS and XPS, Electrochim. Acta. 275 (2018) 265–274. https://doi.org/10.1016/j.electacta.2018.04.114.

[18] A.L. Giraldo, E.D. Erazo-Erazo, O.A. Flórez-Acosta, E.A. Serna-Galvis, R.A. Torres-Palma, Degradation of the antibiotic oxacillin in water by anodic oxidation with Ti/IrO 2 anodes: Evaluation of degradation routes, organic by-products and effects of water matrix components, Chem. Eng. J. 279 (2015) 103–114. https://doi.org/10.1016/j.cej.2015.04.140.

[19] E.A. Serna-Galvis, K.E. Berrio-Perlaza, R.A. Torres-Palma, Electrochemical treatment of penicillin, cephalosporin, and fluoroquinolone antibiotics via active chlorine: evaluation of antimicrobial activity, toxicity, matrix, and their correlation with the degradation pathways, Environ. Sci. Pollut. Res. (2017). https://doi.org/10.1007/s11356-017-9985-2.

[20] Octave Levenspiel, INGENIERÍA DE LAS REACCIONES QUÍMICAS, SEGUNDA, Mexico, 1986.

[21] K.E. Pinkston, D.L. Sedlak, Transformation of aromatic ether- and amine-containing pharmaceuticals during chlorine disinfection, Environ. Sci. Technol. 38 (2004) 4019–4025. https://doi.org/10.1021/es035368l.

[22] W. Sorasuchart, J. Wardrop, J.W. Ayres, Drug release from spray layered and coated drug-containing beads: Effects of pH and comparison of different dissolution methods, Drug Dev. Ind. Pharm. 25 (1999) 1093–1098. https://doi.org/10.1081/DDC-100102274.

[23] M. Deborde, U. von Gunten, Reactions of chlorine with inorganic and organic compounds during water treatment-Kinetics and mechanisms: A

critical review, Water Res. 42 (2008) 13–51. https://doi.org/10.1016/j.watres.2007.07.025.

[24] P. Englezos, N. Kalogerakis, APPLIED PARAMETER ESTIMATION FOR CHEMICAL ENGINEERS, 2001.

[25] E. Serna-Galvis, R.E. Palma, J.E. Ramirez, R.A. Torres, Electrochemical Degradation of Naproxen (NPX) and Diclofenac (DFC) through Active Chlorine Species (Cl 2 -active): Considerations on Structural Aspects and Degradation in Urine, ECS Trans. 100 (2021) 55–71. https://doi.org/10.1149/10001.0055ecst.

[26] E.P. Rivero, F.A. Rodríguez, M.R. Cruz-Díaz, I. González, Reactive diffusion migration layer and mass transfer wall function to model active chlorine generation in a filter press type electrochemical reactor for organic pollutant degradation, Chem. Eng. Res. Des. 138 (2018) 533–545. https://doi.org/10.1016/j.cherd.2018.07.010.

[27] F. Cao, M. Zhang, S. Yuan, J. Feng, Q. Wang, W. Wang, Z. Hu, Transformation of acetaminophen during water chlorination treatment: kinetics and transformation products identification, Environ. Sci. Pollut. Res. 23 (2016) 12303–12311. https://doi.org/10.1007/s11356-016-6341-x.

[28] M. Bedner, W.A. MacCrehan, Transformation of acetaminophen by chlorination produces the toxicants 1,4-benzoquinone and N-acetyl-p-benzoquinone imine, Environ. Sci. Technol. 40 (2006) 516–522.

https://doi.org/10.1021/es0509073.

[29] E.A. Serna-Galvis, J.E. Ramirez, R.E. Palma-Goyes, R.A. Torres-Palma, Indirect electrochemical degradation of acetaminophen: process performance, pollutant transformation, and matrix effects evaluation, Rev. Fac. Ing. In press (2021). https://doi.org/10.17533/udea.redin.20211166.

[30] J.D. Salciccioli, Y. Crutain, M. Komorowski, D.C. Marshall, Sensitivity Analysis and Model Validation, in: M.I.T.C. Data (Ed.), Second. Anal. Electron. Heal. Rec., Springer International Publishing, Cham, 2016: pp. 263–271. https://doi.org/10.1007/978-3-319-43742-2_17.

[31] C.W. Spalding, Reaction kinetics in the absorption of chlorine into aqueous media, AIChE J. 8 (1962) 685–689. https://doi.org/10.1002/aic.690080524.

[32] E.A. Serna-Galvis, K.E. Berrio-Perlaza, R.A. Torres-Palma, Electrochemical treatment of penicillin, cephalosporin, and fluoroquinolone antibiotics via active chlorine: evaluation of antimicrobial activity, toxicity, matrix, and their correlation with the degradation pathways, Environ. Sci. Pollut. Res. (2017). https://doi.org/10.1007/s11356-017-9985-2.

[33] E.A. Serna-Galvis, S.D. Jojoa-Sierra, K.E. Berrio-Perlaza, F. Ferraro, R.A. Torres-Palma, Structure-reactivity relationship in the degradation of three representative fluoroquinolone antibiotics in water by electrogenerated active chlorine, Chem. Eng. J. 315 (2017) 552–561. https://doi.org/10.1016/j.cej.2017.01.062.

[34] M.C. Dodd, A.D. Shah, U. Von Gunten, C.H. Huang, Interactions of fluoroquinolone antibacterial agents with aqueous chlorine: Reaction kinetics, mechanisms, and transformation pathways, Environ. Sci. Technol. 39 (2005) 7065–7076. https://doi.org/10.1021/es050054e.

[35] L.R. Peterson, Quinolone molecular structure-activity relationships: what we have learned about improving antimicrobial activity., Clin. Infect. Dis. 33 (2001) S180–S186. https://doi.org/10.1086/321846.

[36] K.J. Aldred, R.J. Kerns, N. Osheroff, Mechanism of quinolone action and resistance, Biochemistry. 53 (2014) 1565–1574. https://doi.org/10.1021/bi5000564.

[37] J.M. Domagala, Structure-activity and structure-side-effect relationships for the quinolone antibacterials, J. Antimicrob. Chemother. 33 (1994) 685–706. https://doi.org/10.1093/jac/33.4.685.

Declaration of interests

☒ The authors declare that they have no known competing financial interests or personal relationships that could have appeared to influence the work reported in this paper.

☐The authors declare the following financial interests/personal relationships which may be considered as potential competing interests: